Preflight Summary Report for: Phase_Lin.pdf

Profile: Convert to PDF/A-1b (Processed pages 1 to 10)

Processed by Sara Pichette, Date: 12/18/18 2:54 PM

Fixups

- Prepare annotations for PDF/A-1 (314 objects)
- Convert to PDF/A-1b (2 objects)
- Make document XMP Metadata compliant with PDF/A-1 (1 object)
- Remove document structure compression (1 object)
- Compress all uncompressed objects using lossless ZIP compression (1 object)
- Recompress LZW as ZIP (1 object)
- Adjust colors for PDF based ISO standards (1 object)
- Fix font encoding (CIDSet) (1 object)
- Fix font encoding (CharSet) (21 objects)
- Embed fonts (even if text is invisible) (1 object)
- Fix font encoding (CIDToGIDMap) (1 object)
- Remove XMP Metadata if not compliant with PDF/A-1 (1 object)
- Add missing SPACE glyphs (21 objects)
- Repair invalid ToUnicode CMap information in fonts (9 objects)
- Remove compressed XMP Metadata on object level (5 objects)

Results (Summary)

✔ **No problems found**

Document information

File name: "Phase_Lin.pdf"
Path: "/Users/sarapichette/Documents"
PDF version number: "1.4"
File size (MB): 7.8
Title: "Phase-Transfer Ligand Exchange of Lead Chalcogenide Quantum Dots for Direct Deposition of Thick, Highly Conductive Films"
Author: "Qianglu Lin, Hyeong Jin Yun, Wenyong Liu, Hyung-Jun Song, Nikolay S. Makarov, Oleksandr Isaienko, Tom Nakotte, Gen Chen, Hongmei Luo, Victor I. Klimov, and Jeffrey M. Pietryga"
Creator: "Arbortext Advanced Print Publisher 10.0.1465/W Unicode"
Producer: "Acrobat Distiller 8.1.0 (Windows); modified using iText 4.2.0 by 1T3XT"
Created: "5/9/17 1:58 PM"
Modified: "12/18/18 2:52 PM"
Subject: "J. Am. Chem. Soc. 2017.139:6644-6653"
Trapping: "Unknown"
Number of plates: 6
Names of plates: "(Cyan) (Magenta) (Yellow) (Black) (Scheme) (Shading) "

Environment

Preflight, 18.2.0 (201)
Acrobat version: 17.110
Operating system: Mac OS X 10.13.6

JACS
JOURNAL OF THE AMERICAN CHEMICAL SOCIETY
Article
pubs.acs.org/JACS

Phase-Transfer Ligand Exchange of Lead Chalcogenide Quantum Dots for Direct Deposition of Thick, Highly Conductive Films

Qianglu Lin,[†,§] Hyeong Jin Yun,[†,§] Wenyong Liu,[†] Hyung-Jun Song,[†] Nikolay S. Makarov,[†] Oleksandr Isaienko,[†] Tom Nakotte,[‡] Gen Chen,[‡] Hongmei Luo,[‡] Victor I. Klimov,[†] and Jeffrey M. Pietryga*[,†]

[†]Chemistry Division, Los Alamos National Laboratory, Los Alamos, New Mexico 87545, United States
[‡]Department of Chemical and Materials Engineering, New Mexico State University, Las Cruces, New Mexico 88003, United States

Supporting Information

ABSTRACT: The use of semiconductor nanocrystal quantum dots (QDs) in optoelectronic devices typically requires postsynthetic chemical surface treatments to enhance electronic coupling between QDs and allow for efficient charge transport in QD films. Despite their importance in solar cells and infrared (IR) light-emitting diodes and photodetectors, advances in these chemical treatments for lead chalcogenide (PbE; E = S, Se, Te) QDs have lagged behind those of, for instance, II−VI semiconductor QDs. Here, we introduce a method for fast and effective ligand exchange for PbE QDs in solution, resulting in QDs completely passivated by a wide range of small anionic ligands. Due to electrostatic stabilization, these QDs are readily dispersible in polar solvents, in which they form highly concentrated solutions that remain stable for months. QDs of all three Pb chalcogenides retain their photoluminescence, allowing for a detailed study of the effect of the surface ionic double layer on electronic passivation of QD surfaces, which we find can be explained using the hard/soft acid−base theory. Importantly, we prepare highly conductive films of PbS, PbSe, and PbTe QDs by directly casting from solution without further chemical treatment, as determined by field-effect transistor measurements. This method allows for precise control over the surface chemistry, and therefore the transport properties of deposited films. It also permits single-step deposition of films of unprecedented thickness via continuous processing techniques, as we demonstrate by preparing a dense, smooth, 5.3-μm-thick PbSe QD film via doctor-blading. As such, it offers important advantages over laborious layer-by-layer methods for solar cells and photodetectors, while opening the door to new possibilities in ionizing-radiation detectors.

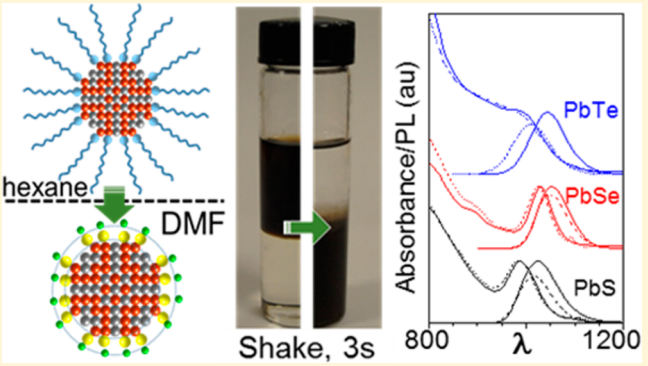

INTRODUCTION

Semiconductor nanocrystal quantum dots (QDs) are of interest for use in a range of optoelectronic device applications that seek to take advantage of their size-tunable optical properties and amenability to low-cost solution-based processing.[1] With their optical absorption and emission being tunable over a wide range of energies spanning from the near- to mid-infrared (mid-IR), lead chalcogenide (PbE; E = S, Se, or Te) QDs have been the materials of choice for applications such as IR photodetectors[2] and light-emitting diodes (LEDs),[3] as well as for photovoltaics.[4] In addition, as with other materials based on lead, the high stopping-power of PbE QDs render them of great interest for use in high-energy ionizing-radiation detectors.[5]

The use of chemically synthesized QDs in electronic devices typically requires the ability to transport charge carriers (electrons and holes) between QDs within an extended solid.[6] The desired distance of efficient charge transport varies with the application, from ca. 10 nm for LEDs,[7] to ca. 1 μm for a solar cell,[8] and to 10−1000 μm for ionizing-radiation (e.g., X-ray or γ-ray) detectors.[9] In these latter cases, this requires overcoming the complications imposed by QD ligands, which are typically highly insulating, long-chain organic surfactants.[10]

For PbE QD-based devices, chemical replacement of the original ligands by shorter molecules or ions is carried out invariably during deposition of the QD solid.[6] In the "layer-by-layer" (LbL) approach, as-synthesized PbE QDs are dip- or spin-coated onto a substrate and are subsequently exposed to a solution containing a large excess of short ligands such as hydrazine[11] or 1,2-ethanedithiol.[10] The finite penetration depth of the exchange solution, as well as the need to accommodate the volume change resulting from the exchange, imposes a limit on the thickness that can be deposited in one step, which is typically only up to a few tens of nanometers. Thicker layers require time-consuming and cumbersome iterations of the process,[12] reexposing already deposited layers to solvents and

Received: February 7, 2017
Published: April 21, 2017

DOI: 10.1021/jacs.7b01327
J. Am. Chem. Soc. 2017, 139, 6644−6653

chemicals, potentially causing physical damage and compositional mixing between layers in junction structures. Typically, due to the accumulation of physical defects, LbL-deposited PbE QD films of thickness >800 nm (>50 layers) are prone to cracking and delamination. This is still below the thickness required for fully capturing the solar spectrum, let alone for ionizing-radiation detection.

An attractive alternative is to perform ligand exchange completely in solution first, followed by spin-coating or dip-coating QDs onto substrates. Decoupling ligand exchange from deposition offers the potential for thicker, more homogeneous films and the possibility of using advanced methods, like spray-coating, electrophoretic deposition, or doctor-blading, that do not lend themselves to the sequential chemistry of the LbL approach. In-solution ligand exchange of QDs with short ligands and ions has been demonstrated for a number of systems, and is often accomplished by a biphasic approach that brings the surface-exchanged QDs into a polar solvent in which the colloidal stability relies to a large degree on electrostatic forces.[6,13] To date, the most success has been achieved in colloidal ligand exchange of cadmium chalcogenide QDs with metal−chalcogenide complexes,[14] metal-free inorganic ligands,[15] and composition-matched solder ligands.[13c] Such methods have been used to fabricate QD field-effect transistors (FETs) that, after sintering, demonstrated carrier mobilities close to those of bulk semiconductor.[16]

Because of their uniquely sensitive surfaces,[17] in-solution ligand exchange of PbE QDs has proven more challenging, although there are a few reported successes for specific pairings of QD and ligand, including using lead iodide-based ligands with PbS or PbTe QDs.[13a,b] Though no device fabrication was carried out in these cases, recently, similarly prepared PbS QDs were used as one layer within an LbL-deposited solar cell with a power conversion efficiency of nearly 9%.[18] In-solution ligand exchange with ammonium iodide (NH_4I) was also used in the preparation of a photovoltaic device based on PbS QDs,[19] and as the first step to create FETs based on PbSe QDs that, after infilling with alumina (Al_2O_3) via atomic-layer deposition (ALD), exhibited *n*-type mobilities of ∼2 $cm^2/(V\,s)$,[20] approaching the highest reported values for ALD-coated PbSe QD FETs.[21] These examples are promising, but given the potential for controlling the carrier properties of, for example, PbS QDs through surface exchange,[22] they collectively only hint at the potential power of a truly universal method for performing in-solution ligand exchange on PbE QDs of all compositions and with arbitrary choice of short ligand.

Here, we demonstrate a universal protocol for fast, quantitative ligand exchange and phase transfer of PbS, PbSe, and PbTe QDs using a wide range of small, ionic ligands including halides, pseudohalides, and carboxylates. The key is the combined use of a synthesis that produces QDs initially featuring weakly bound oleylamine (OLA) ligands, and nonoxidizing yet highly polar solvents, including the relatively low-boiling 2,6-difluoropyridine (DFP). In addition to its unmatched versatility, compared to reported colloidal ligand exchange of PbE QDs, quantitative exchange by our process takes seconds instead of hours of reaction time.[13b] The resulting electrostatically stabilized dispersions, for many ionic ligands, can be surprisingly stable (resisting aggregation/precipitation for months) over a wide range of concentrations (up to ∼100 mg/mL). Interestingly, the photoluminescence (PL) efficiencies of QDs in polar dispersions are strongly dependent not only on the identity of the anion passivant but also on its accompanying counterion, from which we infer variations in the efficacy of electronic passivation that can be understood using hard/soft acid−base (HSAB) theory.[23] Finally, we use our new method to fabricate FET and simple photodetector devices based on physically robust, high-quality PbS, PbSe, and PbTe QD films of arbitrary thickness of up to several micrometers, cast in a single step. Through analysis of the performance of these devices, we demonstrate how charge carrier properties in our QD films can be widely tuned through choice of ligand, thermal annealing, and inclusion of additional coligands.

EXPERIMENTAL METHODS

General Considerations. Lead bromide ($PbBr_2$, 99.999%), tellurium shot (Te, 99.9999%), selenium shot (Se, 99.999%), sulfur powder (S, 99.5%), and 2,6-difluoropyridine (DFP, 98+%) were purchased from Alfa Aesar; oleylamine (OLA, 80−90%), 1-octadecene (ODE, 90% tech.), lead(II) iodide (99%), tri-*n*-butylphosphine (TBP, 95%), *N*,*N*-dimethylformamide (DMF, 99+%), *N*-methylformamide (NMF, 99+%), lithium thiocyanate hydrate (LiSCN, 99%), and formamide (FA, 99.6%) were purchased from Acros Organics; chloroform (HPLC grade) and hexane (HPLC grade) were purchased from Fisher Chemical; tri-*n*-octylphosphine (TOP, 97%) and di-*n*-isobutylphosphine (DIP, 97%) were purchased from Strem Chemicals; tris(diethylamino)phosphine (TDP, 97%), formic acid (HCOOH, 98%), lithium formate monohydrate (LiOOCH, 98%), acetonitrile (anhydrous, 99.8%), lithium iodide (LiI, anhydrous, 99.999%), lithium bromide (LiBr, anhydrous, 99.999%), potassium iodide (KI, anhydrous, 99%), sodium iodide (NaI, anhydrous, 99.999%), cadmium iodide (CdI_2, anhydrous, 99.999%), and potassium selenocyanate (KSeCN, 99%) were purchased from Sigma-Aldrich. Prediced silicon/silicon oxide substrates were purchased from Ossila Ltd. TOPSe (2 M) solution was prepared by stirring 10 mmol Se shot in 5 mL of TOP in a N_2-filled glovebox until dissolved. OLA-S (0.5 M) was prepared by stirring 5 mmol S powder in 10 mL of OLA at 80 °C in a N_2-filled glovebox until dissolved. TBPTe (1 M) solution was prepared by stirring 5 mmol Te shot in 5 mL of TBP until dissolved. All reactions were performed under air-free conditions using standard Schlenk and glovebox techniques.

Synthesis of PbSe QDs. In a typical reaction, a three-neck flask is charged with 8 mmol of $PbBr_2$, 8 mL of OLA, and 16 mL of ODE and heated under vacuum at 110 °C for 30 min to obtain a clear solution Then the flask is filled with N_2 and the temperature is raised to 180 °C. A mixture comprising 0.1 mL of DIP, 2 mL of OLA, and 1 mL of 2 M TOPSe is injected into the lead precursor solution. The flask is removed from heat immediately after the injection and allowed to come to room temperature. PbSe QDs 5.0 nm in diameter are obtained. Other sizes can be obtained by lowering the reaction temperature (smaller) or increasing the heating time (larger).

Synthesis of PbS QDs. In a typical reaction, a three-neck flask is charged with 8 mmol of $PbBr_2$ and 10 mL of OLA and heated under vacuum at 110 °C for 30 min to obtain a clear solution. The flask is then filled with N_2, and the temperature is raised to 120 °C. Four milliliters of 0.5 M S-OLA solution is then injected into the flask. After 10 min, the flask is removed from heat and allowed to come to room temperature. PbS QDs 5.8 nm in diameter are obtained.

Synthesis of PbTe QDs. In a typical reaction, a three-neck flask is charged with 8 mmol of $PbBr_2$, 8 mL of OLA, and 16 mL of ODE and heated under vacuum at 110 °C for 30 min to obtain a clear solution. The flask is then filled with N_2 and heated to 180 °C, whereupon 2 mL of 1 M TBPTe is injected into the lead precursor solution. After 10 min at 160 °C, the flask is removed from heat and allowed to come to room temperature. PbTe QDs 5.6 nm in diameter are obtained.

Purification of PbS, PbSe, and PbTe QDs. Addition of 30 mL of chloroform and 10 mL of acetonitrile into the reaction solution causes the QDs to precipitate. The precipitate is then isolated by centrifugation, and the supernatant is discarded. The QDs are then redispersed in 5 mL of hexane with sonication. Unreacted lead

DOI: 10.1021/jacs.7b01327
J. Am. Chem. Soc. 2017, 139, 6644−6653

precursors still remaining in the solution can be removed at this point by centrifugation, discarding the precipitate. The supernatant solution is collected and precipitated one more time by adding 15 mL of chloroform and 5 mL of acetonitrile. After centrifugation, the supernatant is discarded and the precipitate is redispersed in nonpolar solvents such as hexane or chloroform.

Ligand Exchange of PbSe QDs with Various Short Ligands. For the biphasic exchange reactions, either hexane/DMF or chloroform/FA solvent combinations are used, and concentrations can be varied; here we describe a typical example of the former. The chosen ionic passivant (e.g., LiI, LiBr, KI, HCOOH, LiOOCH, LiSCN, KSeCN, NaI, CdI_2, PbI_2) is dissolved in 5 mL of DMF, typically at a concentration of 20 mg/mL; sonication can be applied when necessary to speed the dissolution. PbSe QDs in 5 mL of hexane (also typically ~20 mg/mL) are then added, and after shaking 3 s by hand, the PbSe QDs are transferred from the hexane to the DMF layer completely. The hexane layer is then decanted, and 5 mL of toluene or chloroform is added to the solution to precipitate out QDs, which can be collected by centrifugation and decanting of the supernatant. The precipitate can typically be readily dissolved in DFP, although in some cases gentle sonication and/or addition of a small amount of DMF (about 5% of total volume) aids in forming and stabilizing the dispersion.

Ligand Exchange of PbS, PbSe, and PbTe QDs with Halide Ligands. The general conditions described above can be used for PbS and PbTe QDs with minor modifications to accomplish passivation with a range of ionic ligands. Here, we provide a specific example for Li halide passivation. LiI or LiBr solution (1 M) is prepared by dissolving 10 mmol LiI or LiBr solid in 10 mL of FA or DMF. 3 mL of PbE QDs in hexane was layered onto 3 mL of 1 M LiI in DMF. After 3 s of vigorous shaking, the PbE QDs were transferred completely to the DMF layer. The hexane layer was discarded and 5 mL of chloroform was added to the DMF layer to precipitate the PbE QDs. The supernatant containing excess LiI was discarded, and the precipitate was redispersed in a polar solvent such as FA, NMF, or DFP.

Thick PbSe QD Film by Doctor-Blading. A drop of PbSe/KI QDs solution with a concentration of ~60 mg/mL is cast on a silicon wafer precleaned by immersion in piranha solution (30% hydrogen peroxide solution combined with concentrated sulfuric acid in a 1:3 volume ratio), rinsing with deionized water, and drying with a dry N_2 stream. Then a razor blade is used to spread out the solution on the substrate and smooth the surface. After drying at room temperature for 10 min, a 5.3 μm PbSe QD film is obtained.

Fabrication and Characterization of FETs and *C*−*V* Measurement Devices. PbSe QDs FETs were fabricated using heavily *p*-doped silicon wafers with thermally grown silicon oxide (300 nm thickness). The wafers were sonicated in acetone (2 × 10 min) and 2-propanol (1 × 10 min) and then immersed in piranha solution overnight. Residual acid was removed by rinsing twice with deionized water, followed by heating at 200 °C on a hot plate for 30 min to remove residual water. Au source and drain contacts (3 mm channel width and 100 μm channel length) were deposited by thermal evaporation (1 Å/s rate) through a shadow mask to achieve 100 nm thickness. Then PbSe/KI QDs in DFP solution (typically ~40 mg/mL) with 50 mM TDP were spin-coated on the substrate at 2000 rpm for 30 s, followed by annealing on a hot plate (100−200 °C) for 30 min. Preparation of PbS and PbTe QD devices followed the same procedure, without TDP in the QD solution, respectively. Electron mobilities were derived within the linear regime from the slope of the source-drain current (I_{DS}) vs gate voltage (V_{GS}) dependence; the threshold voltage (V_{th}) of each FET was determined by extrapolation of the on-state $I_{DS}^{1/2}$ vs V_{GS} curve biased in the saturation regime. The devices for *C*−*V* measurements were fabricated using the same cleaned Si/SiO_2 substrates. Lead chalcogenide QDs were spin-coated onto the substrate using the same parameters as for FET fabrication, and then a top Au contact (dimensions 3 mm × 5 mm) was deposited by thermal evaporation (~100 nm of thickness) through a mask. The completed devices were annealed at 180 °C for 30 min before measuring capacitance. For *C*−*V* characterization, the top metal contact and the gate are connected to the low and high terminal, respectively, of a capacitance measurement unit. *C*−*V* curves are measured in the range from 100 Hz to 5 kHz; representative *C*−*V* data obtained at 1 kHz are provided in Figure S11 of the Supporting Information (SI). The total charge injected for a given gate voltage (V_g) was calculated from $Q = \int_{V_{th}}^{V_g} C(V_g)\, dV_g$.[24]

Fabrication of PbSe QD Photodetector. PbSe QDs of diameter 2.5 nm with NH_4I passivation are prepared according to the methods above. ITO glass is cleaned with sonication in acetone for 10 min, followed by ozone cleaning for another 10 min. Then PbSe QDs with concentration ~50 mg/mL are spin-coated onto an ITO glass substrate at 300 rpm for 10 min in a N_2-filled glovebox. After annealing the QD film at 80 °C for 10 min, the top Au contact is deposited by thermal evaporation (1 Å/s rate) through a shadow mask to achieve 100 nm thickness.

Materials Characterization. Transmission electron microscope (TEM) images were taken using a JEOL 2010 TEM, using QD samples drop cast from a dispersion onto carbon-coated copper grids. Absorption spectra were measured by a PerkinElmer Lambda 950 spectrophotometer, using an integrating sphere attachment for QD films. Near infrared (NIR) PL spectra were taken using a custom-built apparatus. Samples were excited using the mechanically chopped light from a 808 nm laser, and emission was spectrally dispersed using a grating monochromator and recorded using a liquid-N_2-cooled InSb detector with lock-in amplification. The PL quantum yields (QYs) were determined relative to IR-26 (in 1,2-dicholorethane, QY = 0.048 %).[25] Elemental analysis was carried out using a Shimadzu ICPE-9000 inductively coupled plasma optical emission spectrometer (ICP-OES). PL decay traces were measured using a superconducting nanowire single-photon detector (SNSPD), as described previously[26] (800 nm excitation).

Film thickness and morphology were assessed using atomic force microscopy (AFM), conducted with a Dimension FastScan instrument from Bruker and analyzed with ScanAsyst software. Samples were prepared by using a razor blade to scratch the QD film, removing QDs but not scratching the substrate. Measurements were done by placing the cantilever tip near the scratch and scanning an area that encompassed at least one edge of the scratch.

Device Characterization. FET, photodetector and *C*−*V* characterization were conducted using a semiconductor device parameter analyzer (B1500A, Agilent) in a N_2-filled glovebox. The probe contacts were placed onto electrodes using a dc probe positioner (DPP205-M-R-S, Aztec Enterprises, Inc.). For *C*−*V* measurements, the top (metal) and bottom (*p*-type Si substrate) contacts were connected to the low and high terminals, respectively. The *C*−*V* curve for each device was measured at a frequency of 1 kHz. In PbSe photodetector measurements, illumination was provided by a white light LED source with a maximum intensity of 25.9 W/cm^2 that was attenuated using neutral density filters. We used a spring-loaded pin to make a soft contact on the Au contact and measured the current response from the conducting ITO to Au contact in the dark and upon light illumination.

■ RESULTS AND DISCUSSION

PbE QDs were synthesized using a modification of a published method for preparing air-stable QDs[27] via the reaction of lead halides with an appropriate chalcogen complex in OLA (see the Experimental Methods for details). An attractive feature of this approach is that it produces QDs with excellent size control (Figure S1, SI) and lead-dominated surfaces (according to overall stoichiometry measured by ICP-OES; Table S2, SI) without use of the strongly binding oleate ligand. Although PbE QDs featuring the oleate ligand are nearly universally used in previous reports wherein smooth, crack-free films are deposited by solid-state ligand exchange using LbL methods,[10] removal of oleate ligand in solution results in severe QD aggregation, sintering, and necking.[28] The resulting suspensions are colloidally unstable and produce films with poor morphology, although in particular cases this has been mitigated by slowly displacing oleate with moderate-binding-strength ligands over a

DOI: 10.1021/jacs.7b01327
J. Am. Chem. Soc. 2017, 139, 6644−6653

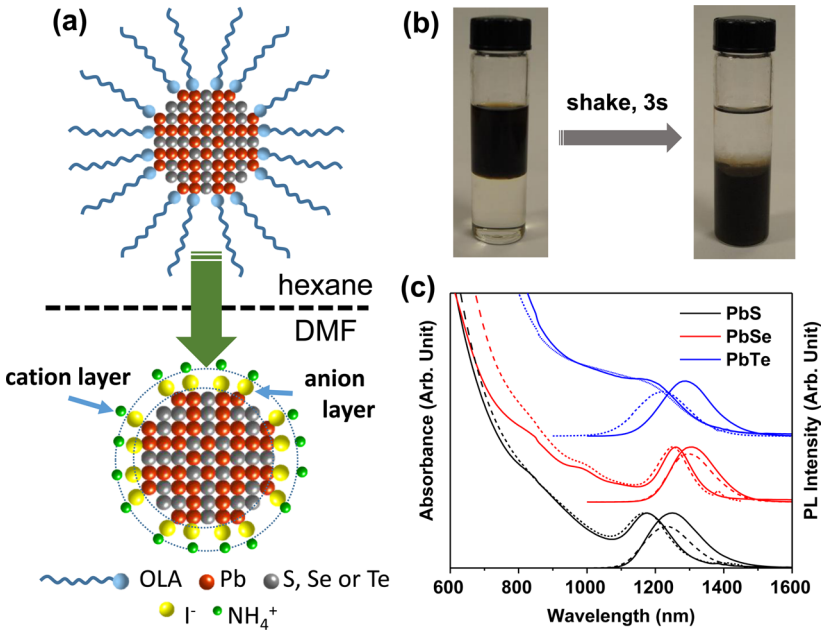

Figure 1. (a) Schematic diagram of the ligand exchange process, showing the transition from hydrophobic/steric to electrostatic stabilization. (b) Photographs of the ligand exchange and accompanying phase transfer of PbSe QDs from hexane (top) to DMF phase (bottom) using NH_4I. (c) Absorption and emission spectra of PbS (4.0 nm, black), PbSe (4.0 nm, red), and PbTe (3.0 nm, blue) QDs before (solid) and after (dashed) ligand exchange with LiI.

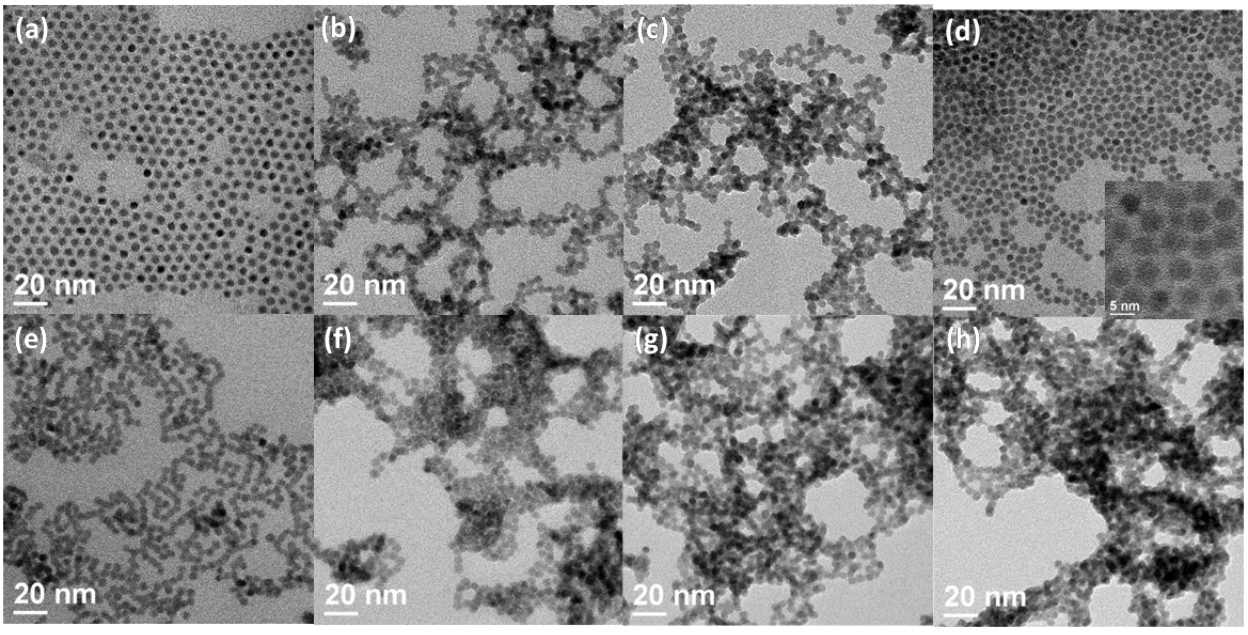

Figure 2. TEM images of 4.4 nm PbSe QDs with various ligands: (a) oleylamine (OLA); (b) potassium iodide (KI); (c) lithium iodide (LiI); (d) lithium bromide (LiBr) (inset: higher resolution image of closely packed PbSe QDs); (e) lithium thiocyanate (LiSCN); (f) potassium selenocyanate (KSeCN); (g) formic acid (HCOOH); and (h) lithium formate (LiCOOH). High-resolution TEM images are shown in Figures S3 and S4 (SI).

period of hours.[13a,b] We find that the lead-rich, oleate-free surfaces of QDs synthesized in OLA make the exchange process much simpler, faster, and reproducible for all PbE QDs in combination with a wide range of ionic ligands. To perform exchange, we used a biphasic approach in which a concentrated ligand solution in polar solvent (e.g., FA, NMF, or DMF; LiI in DMF is shown in Figure 1) is introduced to a hexane solution of QDs, and the mixture is shaken by hand. Within seconds, quantitative ligand exchange occurs, and the anion-passivated QDs are transferred into the polar layer. As shown in Figure 1c, when this method is applied to effect LiI exchange upon PbS, PbSe, and PbTe QDs of similar band gap, transfer occurs with preservation of the principal absorption and PL features (see also Table S1, SI), as well as with minimal effect on PL lifetime (Figure S2, SI).

Using the OLA-synthesized QDs, we were also able to perform equally fast and complete exchange using other small ionic ligands, such as SCN^-, $SeCN^-$, and $HCOO^-$. Although FA, NMF, and DMF, collectively, are suitable for producing complete ligand exchange for all attempted ionic ligands

DOI: 10.1021/jacs.7b01327
J. Am. Chem. Soc. 2017, 139, 6644−6653

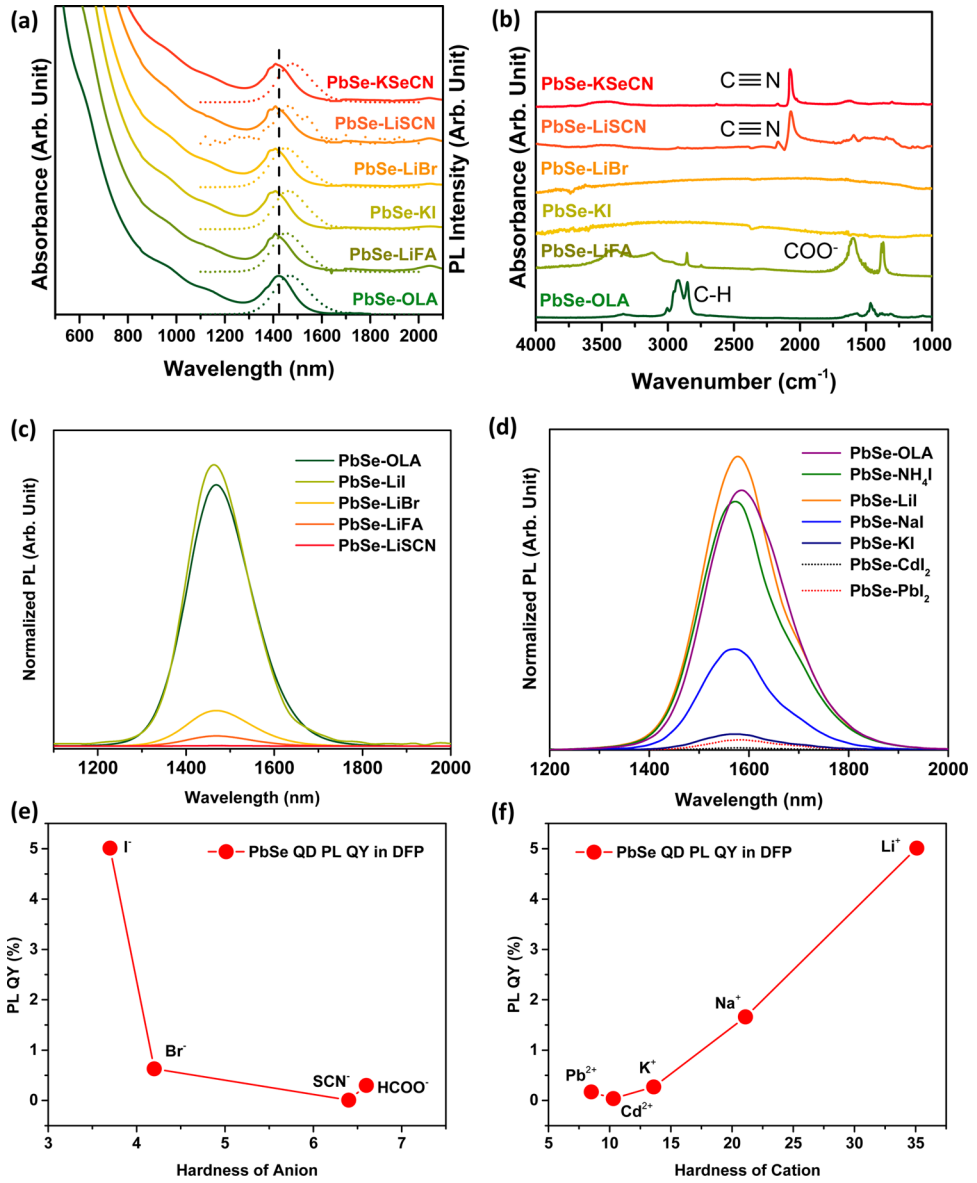

Figure 3. (a) Absorption and PL spectra of 4.4 nm PbSe QDs passivated with OLA, LiOOCH, KI, LiBr, LiSCN, and KSCN (from bottom to top). (b) FTIR spectra of drop-cast films of the 4.4 nm PbSe QDs (a) before and after ligand exchange. (c) PL spectra of DFP solutions of 4.4 nm PbSe QDs after exchange using various Li^+ salts. (d) PL spectra of DFP solutions of 5.0 nm PbSe QDs after exchange using various I^- salts. (e) PbSe QD PL QY with various Li^+ salts as a function of the anion hardness. (f) PbSe QD PL QY with various I^- as a function of the cation hardness. Trends equivalent to those in parts e and f were also observed for FA and DMF dispersions immediately after preparation.

(depending on the solubility of a given ionic precursor in each solvent), they present difficulties for use in film casting. For anions other than halides, QDs were only weakly dispersible in FA and were prone to aggregation over time. Use of NMF, with a higher static dielectric constant (ε = 186 vs 109.5),[29] results in better dispersibility for a wider range of anions, consistent with expectations for electrostatic stabilization.[30,15] However, both FA (201 °C) and NMF (199 °C) have boiling points that make casting of QD films directly from solution difficult, particularly for thick films (>100 nm). On the other hand, DMF was found to be quite suitable for performing the exchange for a wide range of ligands and features a lower boiling point (153 °C), but because of its lower dielectric constant ε = 37.1, QDs eventually aggregate and precipitate out of DMF dispersions. We achieved the best dispersibility and long-term stability using DFP, which combines a relatively low boiling point of 124 °C with ε = 107.8.[31] Thus, in our standard method, after performing exchange using a DMF solution of ionic ligand, complete precipitation of QDs is hastened by addition of chloroform or toluene, and then the QDs are redispersed in DFP for optical studies and/or film deposition. With DFP, we are able to disperse PbSe QDs with, for example, SCN^-, $SeCN^-$, $HCOO^-$, Br^-, and I^- ligands at concentrations up to 100 mg/mL.

Figure 2 contains TEM images of 4.4 nm diameter PbSe QDs before (Figure 2a) and after (Figure 2b–h) ligand exchange. With the original OLA passivation, QDs generally form roughly hexagonal close-packed domains in which QDs are ~2 nm apart, consistent with expectations based on the length of the OLA molecule.[32] After ligand exchange, the spacing between QDs is greatly reduced; in fact, strong attraction between QDs as the solvent evaporates from the

DOI: 10.1021/jacs.7b01327
J. Am. Chem. Soc. 2017, 139, 6644–6653

TEM grid causes them to coalesce into clusters (Figure 2f–h) or "necklace"-type structures [Figures 2e and S3c (SI)].

In Figure 3a, we compare the absorption and normalized PL spectra of 4.4 nm diameter OLA-passivated PbSe QDs in hexane (black) to the same QDs in DFP after exchange with a variety of ionic ligands. In each of the cases shown, the principal absorption and PL features are very slightly shifted to shorter wavelengths, typically by ≤20 nm (≤12 meV). This type of blue-shift could be indicative of a size reduction due to loss of QD surface lead ions; in this size regime, it would correspond to a change in diameter of less than 1 Å (compared to the thickness of a monolayer, 3.1 Å). Elemental analyses of these samples (Table S2, SI) reveal that the Pb:Se ratio indeed decreases with ligand exchange, from 1.30 in the original QDs sample to 1.14–1.29, depending on the ligand, consistent with preferential etching of Pb^{2+} cations from the QD surface. The use of specifically lead- or selenium-containing ligand precursors, as expected, has a more direct impact on the Pb:Se ratio: exchange using PbI_2 slightly increases the ratio, while use of KSeCN dramatically reduces it to below 1. In either of these cases, spectral features remain essentially unshifted (Figure S5, SI), suggesting that etching is prevented during the change in passivation. For all ligands, the completeness of exchange can be verified by using Fourier transform infrared (FTIR) spectroscopy (Figure 3b) to determine the intensity of the C–H stretch signatures of OLA near 2900 cm^{-1}. We attribute the effectiveness of our ligand exchange procedure to the affinity the Pb^{2+}-rich QD surface has for negatively charged ligands when passivated by neutral, easily displaced OLA. In contrast, attempts to perform ligand exchange by this method on PbSe QDs capped with negatively charged oleate ligands were generally unsuccessful even after hours of vigorous stirring.

Because of its simplicity and wide applicability, this method offers the ability to survey the effects of surface chemistry on QD optical properties, such as PL QY, allowing us to look for subtle effects in a way never before possible for PbE QDs. In Figure 3c, we compare the PL spectra of DFP solutions of 4.4 nm PbSe QDs featuring a variety of anionic ligands using the common counterion Li^+. Consistent with general expectations for colloidal QDs, the identity of the anionic ligand, which is bound directly to the QD surface, has a strong effect on emission efficiency (as PL QY; see Table S2, SI). More surprising, however, is the effect of the counterion involved in ligand exchange: in Figure 3d, we see that the PL efficiency of I^--passivated QDs varies with cation over just as wide a dynamic range as with the anion.

Often, the negative impact of a surface ligand on the PL QY can be attributed to the introduction of an electronic state that is capable of trapping a photoexcited carrier. When applying this model to anionic ligands, one would expect to find a correlation between a ligand's effect on PL QY and its oxidation potential, as an indicator of hole-trapping driving force. For example, based on its more favorable oxidation potential, I^- ($2I^- \rightarrow I_2 + 2e^-$: $E_o = -0.535$ V) would be expected to be a stronger hole trapping agent than Br^- ($2Br^- \rightarrow Br_2 + 2e^-$: $E_o = -1.066$ V), and therefore, I^--passivated QDs should have lower PL QY than Br^--passivated QDs. As we see from Table S2 (SI), the opposite is found experimentally. Moreover, this model does not lend itself to explicating the pronounced effect of counterion identity on PL QY. We also note that a previous study of ionically stabilized CdSe QD suspensions have also noted a sensitivity of PL QY to the identity of counterions in solution; although a correlation between PL QY and measured values of QD ζ-potential was observed, it did not lead to a definitive understanding of the true role of cations.[33]

We suggest a plausible explanation for all these dependencies that is related to the electrical double layer that is believed to form on these QDs in polar solution (Figure 1a), which is the key to their electrostatic stabilization against aggregation.[30,34] The interaction strength between cations and anions can be qualitatively,[35] and even semi-quantitatively,[23] predicted by the hard–soft Lewis acid and base (HSAB) model. According to this model, acids and bases can be categorized as "hard" or "soft" based on size, total charge, and other considerations; further, the strongest interactions should occur between acids and bases of the same relative hardness (i.e., hard acids should bind most strongly to hard bases). The hardness of ions, η, can be quantified as $\eta = 1/2(I - A)$, where I and A are the ionization potential and electron affinity of the species.[23] We can apply this model in our case to predict the strength of the interaction between each anion and either the QD surface Pb^{2+} cations or the outer sphere cations of the electrical double layer, respectively. For instance, the soft base I^- interacts strongly with soft acid Pb^{2+} cations, resulting in very effective passivation of the PbSe QD surface and a higher PL QY (Figure 3c). In contrast, we would expect that the formate ion ($HCOO^-$), as a hard base, should be very weakly bound to Pb^{2+}, resulting in low PL QY, as observed. Interestingly, we see even poorer emission efficiency after passivation with the ambidentate SCN^- ligand; this suggests that its interaction is relatively weak, consistent with it adopting an "N-bound" connectivity (rather than S-bound), supporting previous spectroscopic observations in PbS QDs.[36] When we compare the PL QY of PbSe QD samples after exchange with various anions introduced as the lithium salt (Figure 3e, Table S3, SI), we observe that the PL decreases as the anion hardness increases, which fits well with the HSAB model.

The equally strong dependence of PL QY on cation implies that competition between the QD surface and counterions impacts the overall effective anion binding strength. In Figure 3d,f, we see that for (soft base) I^--passivated 5.0 nm PbSe QDs, the hardest acid cations, Li^+ and NH_4^+, result in the highest PL QYs, while soft acids like Cd^{2+} and Pb^{2+} produce the lowest (Tables S2 and S4, SI). This suggests that a stronger interaction between the cation and the I^- anion actually weakens its binding to the QD surface, resulting in less effective passivation and lower PL QY. The particularly dramatic reduction in QY for the two dications studied was reflected in the PL decay traces (Figure S6, SI), which revealed the emergence of a fast, nonradiative relaxation channel. This observation is surprising, as in nonpolar solutions, adding excess lead[17] or cadmium ions[37] to the surface of PbSe QDs generally enhances emission efficiency. This highlights the different factors at play in polar solutions of electrostatically stabilized QDs, specifically a dynamic competition within the electrical double layer in which anions engage in binding interactions of constantly changing strength with the QD surface and the outer-sphere cations (Figure 1a).

As stated above, a key benefit of using DFP as solvent is that its relatively low boiling point allows for single-step casting of films of highly coupled QDs. To demonstrate this, we prepared a 377-nm-thick PbSe/NH_4I QD film using a single spin-coating step. We observed a red-shift in the first absorption peak from 1385 nm in solution to 1405 nm in film (Figure S7a, SI), consistent with enhanced coupling between QDs due to short

DOI: 10.1021/jacs.7b01327
J. Am. Chem. Soc. 2017, 139, 6644–6653

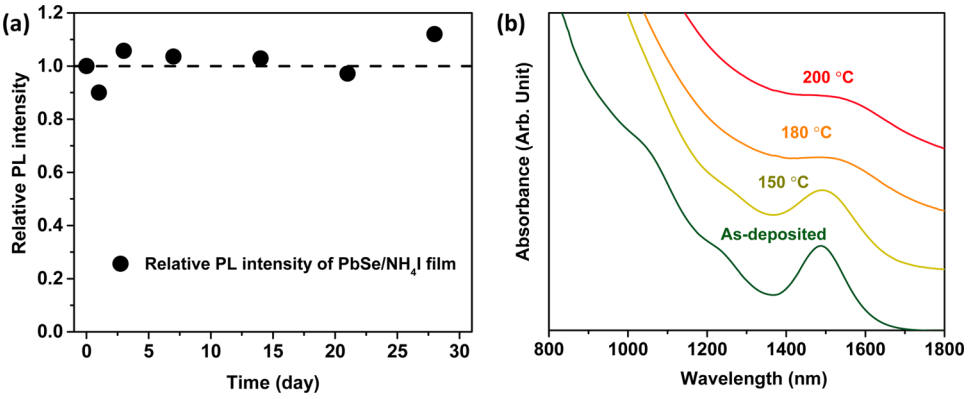

Figure 4. (a) Air stability test of 4.4 nm PbSe/NH_4I QDs film stored in air by measuring relative PL intensities (the dashed line is a guide to the eye with a value of 1). (b) Absorption spectra of PbSe/KI QDs film as-deposited (dark green) and annealed at 150 °C (yellow), 180 °C (orange), and 200 °C (red) for 30 min, respectively.

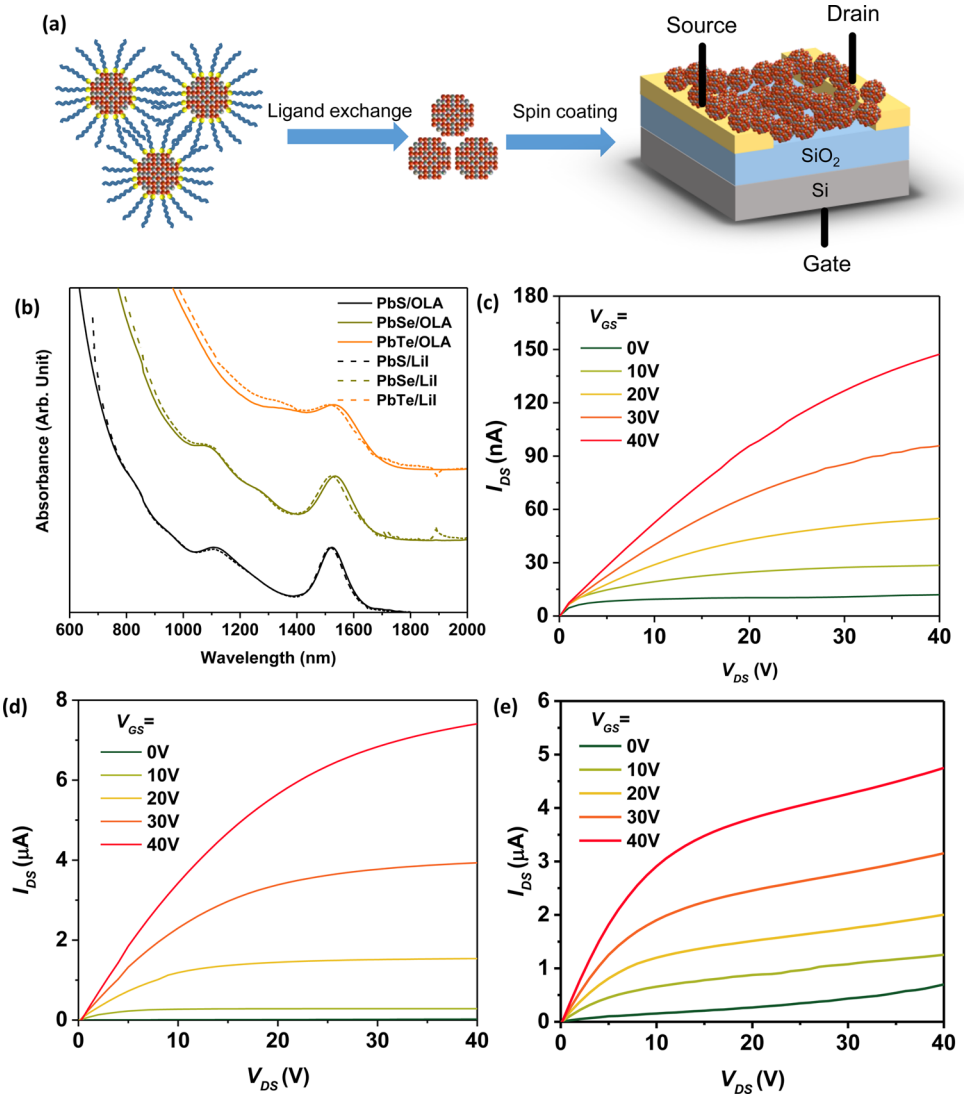

Figure 5. (a) Schematic of FET devices with ionic ligand passivated PbSe QDs. (b) Absorption spectra of PbS (5.8 nm, black), PbSe (5.0 nm, dark yellow), and PbTe (5.7 nm, orange) QDs with similar band gap before (solid, in TCE) and after (dashed, in DFP) ligand exchange with LiI. $I_{SD}-V_{SD}$ curves of PbS/LiI QD FET (c), PbSe/LiI QD FET (d), and PbTe/LiI QD FET (e).

interparticle spacing. Halide passivation has been noted in several reports to enhance the stability of PbSe QDs against oxidation in air;[17,27,38] indeed, we find that both the absorption and the weak near-IR emission at 1480 nm of these films remain unchanged for weeks in air [Figures 4a and S7b (SI)].[17] Inter-QD coupling in these films can be further enhanced by

DOI: 10.1021/jacs.7b01327
J. Am. Chem. Soc. 2017, 139, 6644−6653

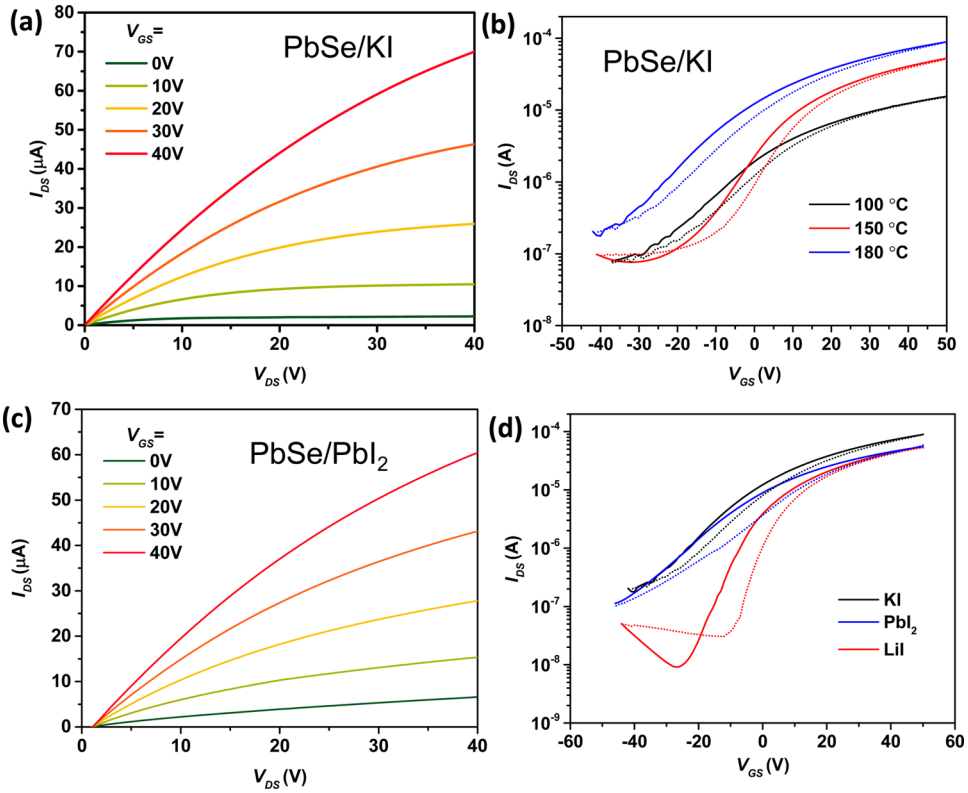

Figure 6. (a) $I_{SD}-V_{SD}$ curves of 5.0 nm PbSe/KI QD FET annealed at 150 °C for 30 min. (b) Transfer curves of PbSe/KI QD FET (at 20 V) annealed at 100 °C (black), 150 °C (red), and 180 °C (blue) for 30 min. (c) $I_{SD}-V_{SD}$ curves of PbSe/PbI_2 QD FET annealed at 150 °C for 30 min. (d) Transfer curves (at 20 V) of PbSe/KI, PbSe/PbI_2, and PbSe/LiI QD FET.

mild annealing: as a PbSe QDs film is heated progressively up to 200 °C, the recognizable shape of a QD absorption spectrum is preserved, while the principal absorption feature broadens and shifts slightly to the red (Figure 4b). This evolution can be understood as resulting from stronger interparticle coupling in these QD film, as has been seen in annealing studies of CdSe QD films,[39] as well as studies of the effects of ligand exchange on coupling in PbSe QD films.[21]

This enhanced coupling should manifest as substantially improved charge carrier transport in QD films and, further, as enhanced performance in QD-based electronic devices. To study the carrier transport properties of lead chalcogenide QD films, we prepared a series of FET devices based on PbE QDs with small ionic ligands (Figure 5a), with Au as source and drain electrodes and a heavily *p*-doped silicon gate topped with 300 nm SiO_2 dielectric. For the sake of comparison, we synthesized PbS, PbSe, and PbTe QDs of very similar band gap (~0.81 eV) and performed ligand exchange using LiI (Figure 5b). Smooth, uniform films (~50 nm in thickness) of each QD were spin-coated from DFP solution and annealed using a slow ramp from 100 to 180 °C for 30 min to evaporate residual solvent and improve QD coupling; no further film treatment was applied. All devices based on LiI-exchanged QDs demonstrated *n*-type transport behavior, with typical electron mobilities of 2.9×10^{-4} $cm^2/(V\ s)$ for PbS (Figure 5c), 0.032 $cm^2/(V\ s)$ for PbSe (Figure 5d), and 0.034 $cm^2/(V\ s)$ for PbTe (Figure 5e). FET transfer characteristics ($I_{DS}-V_{GS}$) measured at V_{DS} of 20 V are shown in Figure S8 (SI). Devices based on LiI-exchanged PbSe QDs exhibited the best on−off switching behavior, with an on−off ratio of $\sim 10^4$ and small hysteresis (ΔV_{th} = 5.87 V) between forward and backward scans. In addition, the PbTe QD FET is particularly noteworthy, as PbTe QDs are the most promising material for "carrier multiplication"-enhanced solar cells.[40] Moreover, to our knowledge, the only previous report of a PbTe QD FET employed postdeposition treatment with hydrazine and resulted in a heavily doped film exhibiting quasi-metallic transport behavior.[41] In contrast, the response of our PbTe QD device after mild annealing is similar to those of PbSe and PbS QD devices; interestingly, annealing at higher temperatures increases mobility dramatically but also results in near-metallic *I*−*V* characteristics similar to that seen in the hydrazine-treated films (Figure S9, SI).[41] This result suggests that changing the annealing temperature and duration is an alternative way to control the doping level of PbTe QD films prepared by this single-step method.

An additional advantage of the single-step casting of coupled QD films via this approach is that it affords the opportunity to include additional coligands, and potentially dopants, within the films simply by adding them to the solution. Extensive experiments on the effects of such additives on carrier transport are ongoing, but in one particularly notable example, it was found that adding a small amount of tris(diethylamido)-phosphine (TDP) to the PbSe QD solution shortly before casting resulted in an order of magnitude enhancement of electron mobility, up to 0.2 $cm^2/(V\ s)$ (Figure S10, SI). To our knowledge, this is a record for single-component PbSe QD films without atomic-layer deposition (ALD) coating.[21] This particular ligand had been used previously to instigate the growth of PbSe nanorods by oriented attachment,[42] suggesting it may enhance crystal-face-specific QD−QD interactions in solution; here, the retention of such interactions in the cast film

DOI: 10.1021/jacs.7b01327
J. Am. Chem. Soc. 2017, 139, 6644−6653

could be responsible for increased mobility. Interestingly, the similar addition of TDP to PbS or PbTe QD films does not result in any enhancement and instead typically reduces electron mobility.

Annealing of PbSe and PbS QD devices enhanced carrier mobility without any appreciable effect on the shape of the $I-V$ response curve, as is demonstrated for a KI-exchanged PbSe QD device (with TDP; Figure 6a,b). The electron mobility after 30 min of thermal annealing at 100 °C is 0.05 $cm^2/(V\ s)$, but it increases to 0.31 $cm^2/(V\ s)$ after annealing at 180 °C. As in the case of solution PL QY, the wide applicability of this film-casting method makes it well-suited to a study of the effect of chemistry on carrier transport. In an example of this, in Figure 6d we show the transfer curves of three equivalent devices employing the same PbSe QDs after exchange with LiI, KI, and PbI_2. In contrast to the effects on PL, the cation identity seems to have a minor effect on electron transport, with all mobilities varying only from 0.17 to 0.31 $cm^2/(V\ s)$ (Table S5, SI). Additionally, preliminary measurements of the carrier concentration of these n-type films were performed using capacitance–voltage measurements (Figure S11 and Table S6, SI) on simple sandwich-type devices using the same Si/SiO_2 substrate and a Au top contact. Concentrations were on the order of $10^{16}-10^{17}$ cm^{-3}, well within the typically observed range for QD films. Although there is no clear correlation between the nature of the cation and carrier concentration, the PbI_2-treated film, which was the most lead-rich in stoichiometry (Table S2, SI) exhibited the highest carrier concentration of 7.5×10^{17} cm^{-3}, which is consistent with the expected effect of Pb:Se ratio on carrier concentration.[43]

The ligand exchange protocol presented here allows for simple, one-step deposition of films of highly coupled PbE QDs wherein thickness can be controlled by modifying deposition parameters (in the case of spin-coating, solution concentration and spin rate, for example), rather than by sequential iteration of multiple steps. This should result in much better compositional uniformity in single layers of significant thickness (>100 nm). It also greatly simplifies the preparation of the more complex multilayer junctions being investigated for QD solar cells and reduces the potential for the intermixing of layers by avoiding the exposure of previous layers to concentrated ligand-exchange solutions. Moreover, because stable QD dispersions of very high concentration (~100 mg/mL) are possible, the range of achievable thicknesses is greatly expanded, opening up completely new possibilities.

Using this new method, we fabricated a simple ITO/PbSe QD/Au sandwich-structure photodetector (Figure S12, SI). PbSe QDs with band gap of 1.1 eV, which correspond to a size of 3.5 nm in diameter, were exchanged with NH_4I ligand and spin-coated on ITO glass substrate and annealed at 80 °C for 30 min. The obtained film is free from cracks according to optical microscopy; from AFM imagery, we determine a film thickness of 313 nm, with a root-mean-square roughness of 19 nm. Upon illumination of various intensities of white light through the glass side of the device, we observed significant enhancement of current under applied bias (Figure S12c, SI). Unlike the FET devices, in which conductivity occurs only in a nanoscopically thin channel, this simple photoconductive device demonstrates that the ligand exchange protocol is effective throughout the thickness of the deposited layer. This implies that, as a departure from layer-by-layer film deposition, its efficacy is essentially independent of film thickness and that it will enable fabrication of much thicker device active layers. For instance, while spin-coating was used for preparing the FETs studied above, we were also able to prepare a dense, smooth, 5.3-μm-thick film of PbSe 4.8 nm QDs in one deposition step using doctor-blading (Figure S13, SI), a continuous method compatible with, e.g., roll-to-roll processing. Such a thickness begins to enter the realm necessary for detection of ionizing radiation,[5] an area of great untapped potential, particularly for lead-based QDs.

CONCLUSION

We developed a fast, efficient, in-solution ligand exchange protocol for replacing the native long-chain ligands of lead chalcogenide QDs with a wide range of small anions. It produces polar QD solutions with excellent colloidal stability and PL QY of the QDs (dependent on the ligand). By surveying a variety of ligand exchange salts, we uncover how, in polar solution, a competition between the binding of anionic ligands to the QD surface and to counterions in the electrical double layer surrounding each QD impacts their efficacy as passivating agents. These polar solutions are then used for single step deposition of electrically coupled QD films. Through preliminary FET measurements, we have demonstrated high mobilities for devices based on QDs of all three lead chalcogenides, including the first PbTe QD FET with saturable $I-V$ response, and a record high mobility for a single-component PbSe QD device. Further detailed studies of the impact of ligand on charge carrier mobilities and concentrations toward realizing a universal understanding of the effect of surface chemistry on PbE QD device performance are ongoing. Finally, we demonstrated the single-step deposition of conductive film >300 nm in thickness suitable for use as the active layer in a simple photodetector and the use of doctor-blading to deposit a high-quality 5.3-μm-thick PbSe QD film in a single step, opening the door to new types of applications, such as ionizing-radiation detectors, not accessible through previous layer-by-layer film deposition methods.

ASSOCIATED CONTENT

Supporting Information

The Supporting Information is available free of charge on the ACS Publications website at DOI: 10.1021/jacs.7b01327.

Elemental analysis data, PL QY, high-resolution TEM images, capacitance–voltage scan, AFM image of PbSe QDs and film, and photoconductivity measurements (PDF)

AUTHOR INFORMATION

Corresponding Author

*pietryga@lanl.gov

ORCID

Victor I. Klimov: 0000-0003-1158-3179

Jeffrey M. Pietryga: 0000-0001-5360-4228

Author Contributions

§Q.L. and H.J.Y. contributed equally to this work.

Notes

The authors declare no competing financial interest.

ACKNOWLEDGMENTS

Q.L., N.S.M., and J.M.P. were supported by the Los Alamos National Laboratory Directed Research and Development (LDRD) program. H.J.Y., W.L., H.-J.S., O.I., T.N., G.C., H.L.,

DOI: 10.1021/jacs.7b01327
J. Am. Chem. Soc. 2017, 139, 6644–6653

and V.I.K. were supported by the Center for Advanced Solar Photophysics, an Energy Frontier Research Center funded by the U.S. Department of Energy, Office of Science, Basic Energy Sciences.

REFERENCES

(1) Talapin, D. V.; Lee, J.-S.; Kovalenko, M. V.; Shevchenko, E. V. *Chem. Rev.* **2010**, *110*, 389.
(2) Konstantatos, G.; Howard, I.; Fischer, A.; Hoogland, S.; Clifford, J.; Klem, E.; Levina, L.; Sargent, E. H. *Nature* **2006**, *442*, 180.
(3) Sun, L.; Choi, J. J.; Stachnik, D.; Bartnik, A. C.; Hyun, B.-R.; Malliaras, G. G.; Hanrath, T.; Wise, F. W. *Nat. Nanotechnol.* **2012**, *7*, 369.
(4) Graetzel, M.; Janssen, R. A.; Mitzi, D. B.; Sargent, E. H. *Nature* **2012**, *488*, 304.
(5) Kim, G.; Huang, J.; Hammig, M. D. *IEEE Trans. Nucl. Sci.* **2009**, *56*, 841.
(6) Kagan, C. R.; Murray, C. B. *Nat. Nanotechnol.* **2015**, *10*, 1013.
(7) Lee, E. M.; Tisdale, W. A. *J. Phys. Chem. C* **2015**, *119*, 9005.
(8) (a) Stranks, S. D.; Eperon, G. E.; Grancini, G.; Menelaou, C.; Alcocer, M. J.; Leijtens, T.; Herz, L. M.; Petrozza, A.; Snaith, H. J. *Science* **2013**, *342*, 341. (b) Zhitomirsky, D.; Voznyy, O.; Levina, L.; Hoogland, S.; Kemp, K. W.; Ip, A. H.; Thon, S. M.; Sargent, E. H. *Nat. Commun.* **2014**, *5*, 3803.
(9) (a) Sellin, P.; Vaitkus, J. *Nucl. Instrum. Methods Phys. Res., Sect. A* **2006**, *557*, 479. (b) Cho, T.; Takahashi, E.; Hirata, M.; Yamaguchi, N.; Teraji, T.; Matsuda, K.; Takeuchi, A.; Kohagura, J.; Yatsu, K.; Tamano, T.; et al. *Phys. Rev. A: At., Mol., Opt. Phys.* **1992**, *46*, R3024.
(10) Luther, J. M.; Law, M.; Song, Q.; Perkins, C. L.; Beard, M. C.; Nozik, A. J. *ACS Nano* **2008**, *2*, 271.
(11) Talapin, D. V.; Murray, C. B. *Science* **2005**, *310*, 86.
(12) Crisp, R. W.; Kroupa, D. M.; Marshall, A. R.; Miller, E. M.; Zhang, J.; Beard, M. C.; Luther, J. M. *Sci. Rep.* **2015**, *5*, 9945.
(13) (a) Zhang, H.; Jang, J.; Liu, W.; Talapin, D. V. *ACS Nano* **2014**, *8*, 7359. (b) Dirin, D. N.; Dreyfuss, S.; Bodnarchuk, M. I.; Nedelcu, G.; Papagiorgis, P.; Itskos, G.; Kovalenko, M. V. *J. Am. Chem. Soc.* **2014**, *136*, 6550. (c) Dolzhnikov, D. S.; Zhang, H.; Jang, J.; Son, J. S.; Panthani, M. G.; Shibata, T.; Chattopadhyay, S.; Talapin, D. V. *Science* **2015**, *347*, 425.
(14) Kovalenko, M. V.; Scheele, M.; Talapin, D. V. *Science* **2009**, *324*, 1417.
(15) Nag, A.; Kovalenko, M. V.; Lee, J.-S.; Liu, W.; Spokoyny, B.; Talapin, D. V. *J. Am. Chem. Soc.* **2011**, *133*, 10612.
(16) Jang, J.; Dolzhnikov, D. S.; Liu, W.; Nam, S.; Shim, M.; Talapin, D. V. *Nano Lett.* **2015**, *15*, 6309.
(17) Bae, W. K.; Joo, J.; Padilha, L. A.; Won, J.; Lee, D. C.; Lin, Q.; Koh, W.-k.; Luo, H.; Klimov, V. I.; Pietryga, J. M. *J. Am. Chem. Soc.* **2012**, *134*, 20160.
(18) Yang, Z.; Janmohamed, A.; Lan, X.; Garcia de Arquer, F. P.; Voznyy, O.; Yassitepe, E.; Kim, G.-H.; Ning, Z.; Gong, X.; Comin, R.; Sargent, E. H. *Nano Lett.* **2015**, *15*, 7539.
(19) Kim, S.; Noh, J.; Choi, H.; Ha, H.; Song, J. H.; Shim, H. C.; Jang, J.; Beard, M. C.; Jeong, S. *J. Phys. Chem. Lett.* **2014**, *5*, 4002.
(20) Sayevich, V.; Gaponik, N.; Plötner, M.; Kruszynska, M.; Gemming, T.; Dzhagan, V. M.; Akhavan, S.; Zahn, D. R. T.; Demir, H. V.; Eychmüller, A. *Chem. Mater.* **2015**, *27*, 4328.
(21) Liu, Y.; Tolentino, J.; Gibbs, M.; Ihly, R.; Perkins, C. L.; Liu, Y.; Crawford, N.; Hemminger, J. C.; Law, M. *Nano Lett.* **2013**, *13*, 1578.
(22) Brown, P. R.; Kim, D.; Lunt, R. R.; Zhao, N.; Bawendi, M. G.; Grossman, J. C.; Bulovic, V. *ACS Nano* **2014**, *8*, 5863.
(23) Parr, R. G.; Pearson, R. G. *J. Am. Chem. Soc.* **1983**, *105*, 7512.
(24) (a) Goldberger, J.; Sirbuly, D. J.; Law, M.; Yang, P. *J. Phys. Chem. B* **2005**, *109*, 9. (b) Kang, M. S.; Sahu, A.; Norris, D. J.; Frisbie, C. D. *Nano Lett.* **2011**, *11*, 3887. (c) Oh, S. J.; Berry, N. E.; Choi, J.-H.; Gaulding, E. A.; Paik, T.; Hong, S.-H.; Murray, C. B.; Kagan, C. R. *ACS Nano* **2013**, *7*, 2413.
(25) Semonin, O. E.; Johnson, J. C.; Luther, J. M.; Midgett, A. G.; Nozik, A. J.; Beard, M. C. *J. Phys. Chem. Lett.* **2010**, *1*, 2445.
(26) Sandberg, R. L.; Padilha, L. A.; Qazilbash, M. M.; Bae, W. K.; Schaller, R. D.; Pietryga, J. M.; Stevens, M. J.; Baek, B.; Nam, S. W.; Klimov, V. I. *ACS Nano* **2012**, *6*, 9532.
(27) Zhang, J.; Gao, J.; Miller, E. M.; Luther, J. M.; Beard, M. C. *ACS Nano* **2014**, *8*, 614.
(28) Oh, S. J.; Berry, N. E.; Choi, J.-H.; Gaulding, E. A.; Lin, H.; Paik, T.; Diroll, B. T.; Muramoto, S.; Murray, C. B.; Kagan, C. R. *Nano Lett.* **2014**, *14*, 1559.
(29) Richardi, J.; Krienke, H.; Fries, P. H. *Chem. Phys. Lett.* **1997**, *273*, 115.
(30) Holman, Z. C.; Kortshagen, U. R. *Nano Lett.* **2011**, *11*, 2133.
(31) Abboud, J.-L.; Notari, R. *Pure Appl. Chem.* **1999**, *71*, 645.
(32) Lu, X.; Yavuz, M. S.; Tuan, H.-Y.; Korgel, B. A.; Xia, Y. *J. Am. Chem. Soc.* **2008**, *130*, 8900.
(33) Nag, A.; Chung, D. S.; Dolzhnikov, D. S.; Dimitrijevic, N. M.; Chattopadhyay, S.; Shibata, T.; Talapin, D. V. *J. Am. Chem. Soc.* **2012**, *134*, 13604.
(34) Verwey, E. J. W. *Chem. Rev.* **1935**, *16*, 363.
(35) Pearson, R. G. *J. Am. Chem. Soc.* **1963**, *85*, 3533.
(36) Fafarman, A. T.; Koh, W.-k.; Diroll, B. T.; Kim, D. K.; Ko, D.-K.; Oh, S. J.; Ye, X.; Doan-Nguyen, V.; Crump, M. R.; Reifsnyder, D. C.; Murray, C. B.; Kagan, C. R. *J. Am. Chem. Soc.* **2011**, *133*, 15753.
(37) Pietryga, J. M.; Werder, D. J.; Williams, D. J.; Casson, J. L.; Schaller, R. D.; Klimov, V. I.; Hollingsworth, J. A. *J. Am. Chem. Soc.* **2008**, *130*, 4879.
(38) (a) Woo, J. Y.; Ko, J.-H.; Song, J. H.; Kim, K.; Choi, H.; Kim, Y.-H.; Lee, D. C.; Jeong, S. *J. Am. Chem. Soc.* **2014**, *136*, 8883. (b) Kim, S.; Marshall, A. R.; Kroupa, D. M.; Miller, E. M.; Luther, J. M.; Jeong, S.; Beard, M. C. *ACS Nano* **2015**, *9*, 8157.
(39) Norman, Z. M.; Anderson, N. C.; Owen, J. S. *ACS Nano* **2014**, *8*, 7513.
(40) (a) Padilha, L. A.; Stewart, J. T.; Sandberg, R. L.; Bae, W. K.; Koh, W.-K.; Pietryga, J. M.; Klimov, V. I. *Acc. Chem. Res.* **2013**, *46*, 1261. (b) Semonin, O. E.; Luther, J. M.; Choi, S.; Chen, H.-Y.; Gao, J.; Nozik, A. J.; Beard, M. C. *Science* **2011**, *334*, 1530. (c) Böhm, M. L.; Jellicoe, T. C.; Tabachnyk, M.; Davis, N. J.; Wisnivesky-Rocca-Rivarola, F.; Ducati, C.; Ehrler, B.; Bakulin, A. A.; Greenham, N. C. *Nano Lett.* **2015**, *15*, 7987.
(41) Urban, J. J.; Talapin, D. V.; Shevchenko, E. V.; Murray, C. B. *J. Am. Chem. Soc.* **2006**, *128*, 3248.
(42) Koh, W.-k.; Bartnik, A. C.; Wise, F. W.; Murray, C. B. *J. Am. Chem. Soc.* **2010**, *132*, 3909.
(43) (a) Luther, J. M.; Pietryga, J. M. *ACS Nano* **2013**, *7*, 1845. (b) Padilha, L. A.; Stewart, J. T.; Sandberg, R. L.; Bae, W. K.; Koh, W. K.; Pietryga, J. M.; Klimov, V. I. *Acc. Chem. Res.* **2013**, *46*, 1261.

DOI: 10.1021/jacs.7b01327
J. Am. Chem. Soc. 2017, 139, 6644−6653